



POTSDAM-INSTITUT FÜR
KLIMAFOLGENFORSCHUNG

Originally published as:

Mbouna, S. G. N., Banerjee, T., [Schöll, E.](#) (2023): Chimera patterns with spatial random swings between periodic attractors in a network of FitzHugh-Nagumo oscillators. - Physical Review E, 107, 5, 054204.

DOI: <https://doi.org/10.1103/PhysRevE.107.054204>


Chimera patterns with spatial random swings between periodic attractors in a network of FitzHugh-Nagumo oscillators

S. G. Ngueuteu Mbouna*

Laboratory of Modeling and Simulation in Engineering, Biomimetics and Prototypes, Faculty of Science, University of Yaoundé I, P. O. Box 812, Yaoundé, Cameroon

Tanmoy Banerjee 

Chaos and Complex Systems Research Laboratory, Department of Physics, University of Burdwan, Burdwan 713 104, India

Eckehard Schöll 

*Institut für Theoretische Physik, Technische Universität Berlin, 10623 Berlin, Germany;
Potsdam Institute for Climate Impact Research, 14473 Potsdam, Germany;
and Bernstein Center for Computational Neuroscience Berlin, Humboldt-Universität, 10115 Berlin, Germany*



(Received 13 October 2022; revised 18 March 2023; accepted 21 April 2023; published 4 May 2023)

For the study of symmetry-breaking phenomena in neuronal networks, simplified versions of the FitzHugh-Nagumo model are widely used. In this paper, these phenomena are investigated in a network of FitzHugh-Nagumo oscillators taken in the form of the original model and it is found that it exhibits diverse partial synchronization patterns that are unobserved in the networks with simplified models. Apart from the classical chimera, we report a new type of chimera pattern whose incoherent clusters are characterized by spatial random swings among a few fixed periodic attractors. Another peculiar hybrid state is found that combines the features of this chimera state and a solitary state such that the main coherent cluster is interspersed with some nodes with identical solitary dynamics. In addition, oscillation death including chimera death emerges in this network. A reduced model of the network is derived to study oscillation death, which helps explaining the transition from spatial chaos to oscillation death via the chimera state with a solitary state. This study deepens our understanding of chimera patterns in neuronal networks.

DOI: [10.1103/PhysRevE.107.054204](https://doi.org/10.1103/PhysRevE.107.054204)

I. INTRODUCTION

A multitude of natural phenomena can be explained as macroscopic collective dynamics of many interacting objects [1]. Oscillators models coupled in diverse configurations have been used as a paradigm for such behavior. A much investigated collective behavior of interacting elements is synchronization which can be simply defined as the entrainment of rhythms of interacting elements [2,3]. Since the first report on synchronization by Christiaan Huygens in 1665 [2], the study of this phenomenon has discovered many variants in increasingly complex coupled systems. A particularly intriguing synchronization phenomenon is the chimera state which is a form of partial synchronization where alternating clusters of synchronized elements and desynchronized elements emerge spontaneously. Surprisingly, the chimera state arises in networks of symmetrically coupled identical elements [4] as a consequence of spontaneous symmetry breaking. Over the past few decades, another symmetry-breaking phenomenon has been intensively investigated, namely oscillation death. An oscillation death state is a quenched oscillation state where coupling-induced symmetry-breaking gives rise to inhomogeneous steady states [5,6] (for a recent review on oscillation

quenching in networks and related topics, see Ref. [7]). An important connection between these two symmetry-breaking states, namely chimera and oscillation death, coined as chimera death, was reported for the first time in Ref. [8]; it combines the features of chimera states and oscillation death, i.e., the coexistence of spatially coherent and incoherent regions of steady states. Another symmetry-breaking state that was found more recently is the solitary state, that is a form of partial synchronization where individual solitary oscillators leave the synchronous cluster at random positions in space [9]. Solitary states have been found in oscillator networks of various types [10–15]. Chimera and solitary states are often seen as dynamical scenarios of the transition from completely synchronized behavior to completely irregular behavior [4,14]. In this context, a peculiar partial synchronization pattern has also been reported, namely the solitary state chimera that combines the features of chimera state and solitary state: coexistence of coherent and incoherent domains where the incoherent cluster involves the solitary state [16,17].

In the particular context of neuroscience, synchronization in neuronal networks (including mechanisms of desynchronization) is believed to play a crucial role in explaining the brain functioning under normal and pathological conditions (for a review, see Refs. [18,19]). Specifically, chimera states have been found to explain unihemispheric sleep (where the neurons in the sleepy hemisphere of the brain are

*ngueut@yahoo.fr

synchronized and the neurons in the awake hemisphere are desynchronized) exhibited by certain aquatic mammals and multiple bird species [20,21]. Strong neuronal synchrony among the neurons is believed to produce adverse effects, such as Parkinson's disease [22] and epilepsy [23]. Therefore, the possible transitions from the pathological synchronized regimes to the healthy desynchronized states (or vice versa) can involve hybrid patterns such as chimera states and solitary states [24]. For example, a parallel has been drawn between epileptic seizures and the collapse of the chimera state into a global synchronous state in coupled neurons [25,26]. Therefore, the study of chimera states, solitary states, and solitary state chimeras in neuronal networks is of particular importance in explaining macroscopic brain behavior that would be considered as manifestation of partial synchronization of neurons. On the other hand, the oscillation death phenomenon has been used to interpret the phenomenon of winner-takes-all dynamics in neurons [27]. Overall, the suppression of rhythms in neuronal ensembles suggests a dynamical strategy for rapidly and effectively preventing or even terminating a wide range of deleterious neural activity such as epileptic seizures, Parkinson's disease, and schizophrenia [7].

For the study of brain microscopic dynamical functions, relevant models include Hodgkin-Huxley, Izhikevich, and Rulkov map dynamics, whereas for neuronal ensembles, phenomenological models span FitzHugh-Nagumo, Hindmarsh-Rose, and Kuramoto oscillators [28]. The FitzHugh-Nagumo oscillator is the most widely used model when investigating chimera states and solitary states in brain networks [4,18,19,29]. However, to the best of our knowledge, the original model of the FitzHugh-Nagumo oscillator, which contains the stimulus current intensity (a parameter corresponding to membrane current in the original Hodgkin-Huxley equations) has not yet been considered in this context. This stimulus current intensity term is responsible for various inherent dynamics of the FitzHugh-Nagumo model, such as absence of all-or-none spikes, excitation block, and anodal break excitation [30]. Therefore the natural question arises: How does the original FitzHugh-Nagumo model behave in a network with respect to symmetry-breaking phenomena? In this paper, we aim to investigate the possible symmetry-breaking phenomena in a network of the original FitzHugh-Nagumo model. Apart from the classical chimera state, which was found in the literature, we observe additional symmetry-breaking states. Two novel chimera patterns are observed, namely (i) type-1 chimera, where the incoherent clusters are characterized by spatial random swings among a few fixed periodic attractors, and (ii) type-2 chimera, a peculiar hybrid state that combines the features of type-1 chimera state and a solitary state such that the main coherent cluster is interspersed with some nodes with identical solitary dynamics. We further observe chimera death and multicluster coherent oscillation death states.

In general, depending on how the oscillators are organized in the incoherent cluster, two main types of chimera states have been identified. For the first type, which was historically observed first [31,32], the incoherent cluster is in a spatiotemporal chaos regime while the coherent cluster may either be periodic or remain close to a steady state [33,34]. In the second type, the incoherent cluster is in a spatial chaos regime while the coherent cluster may either be a homoge-

neous steady state or a periodic state [33,34]. In Ref. [35], these first and second types of chimeras was identified as “t-chimera” and “s-chimera,” respectively. As the basic chimera structure, the “t-chimera” state has been extensively studied in various coupled systems (for reviews, see Refs. [4,36]). Contrarily, the “s-chimera” state has been less observed [33,34]. For example “s-chimera” states have found to mediate the transition from complete spatial coherence to spatial chaos in networks of discrete time systems (coupled maps) [37–39]. Besides, in most of the previous works investigating symmetry-breaking phenomena in networks of FitzHugh-Nagumo systems, the prominent patterns found were the “t-chimera” state (see for example Refs. [15,18,19,29,40]), a variant known as coherence-resonance chimera [41–43], and solitary states [14,15,17,44]. A coherence-resonance chimera, obtained in networks of excitable elements under the effect of noise, combines the temporal features of coherence resonance and the spatial features of chimera states. In the coherence-resonance chimeras obtained in networks of excitable FitzHugh-Nagumo systems, the location of coherent and incoherent domains of the “t-chimera” state switch alternately in the course of time. In the present paper we report a form of “s-chimera” state in coupled time-continuous systems, namely type-1 chimera state, whose incoherent cluster involves a particular form of spatial chaos characterized by a phase-fliplike instability. The dynamics of all oscillators converge to a few periodic trajectories that show constant phase lags. The spatial chaos in type-1 and type-2 chimeras found here also look like salt-and-pepper states [45] observed in networks of FitzHugh-Nagumo oscillators under the effect of time delay [46,47]. These novel chimera states are observed for the first time in coupled FitzHugh-Nagumo systems.

II. THE NETWORK MODEL

We consider a ring-network of N identical FitzHugh-Nagumo oscillators where each oscillator is diffusively coupled through the two dynamical variables to its $2R$ neighbors (R on each side). The coupling between two units involves direct and cross couplings between the two variables. This mixed coupling is modeled by a rotational coupling matrix [40]. We consider here the original version of the FitzHugh-Nagumo model of neurons [48]. Let the variables u and v describe the membrane voltage and the coarse-grained action of gating variables, respectively, and σ the coupling strength. Then the network is described by the following set of differential equations:

$$\begin{aligned} \varepsilon \frac{du_k}{dt} &= v_k + u_k - \frac{1}{3}u_k^3 + I \\ &+ \frac{\sigma}{2R} \sum_{j=k-R}^{k+R} [b_{uu}(u_j - u_k) + b_{uv}(v_j - v_k)], \\ \frac{dv_k}{dt} &= -u_k - \delta v_k + \gamma \\ &+ \frac{\sigma}{2R} \sum_{j=k-R}^{k+R} [b_{vu}(u_j - u_k) + b_{vv}(v_j - v_k)], \end{aligned} \quad (1)$$

where $k = 1, 2, \dots, N$, and periodic boundary conditions are assumed, the rotational coupling matrix is given by

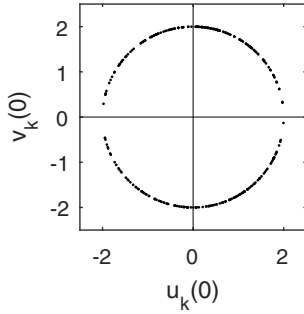


FIG. 1. Initial conditions.

$\begin{pmatrix} b_{uu} & b_{uv} \\ b_{vu} & b_{vv} \end{pmatrix} = \begin{pmatrix} \cos \phi & \sin \phi \\ -\sin \phi & \cos \phi \end{pmatrix}$ with $\phi \in [-\pi, \pi)$ [40], ε is a small parameter responsible for the occurrence of relaxation oscillations, and I is the stimulus intensity, a parameter corresponding to membrane current in the Hodgkin-Huxley equations. The values of the parameters are chosen very close to those considered by FitzHugh in his pioneering work [48], namely $\varepsilon = 0.1$, $\delta = 0.8$, and $\gamma = 0.7$. The parameter I was considered in Ref. [48] as a control parameter to determine the number of equilibrium points and whether the system is in the excitable or oscillatory regime. In the present work, the value of I is set at -0.5 such that each uncoupled FitzHugh-Nagumo oscillator exhibits oscillatory behavior (relaxation oscillations) around only one equilibrium point.

If one applies the transformation $v \rightarrow -v$ and sets $I = \delta = 0$ in Eq. (1), then one uncovers another version of the network model with the simplified FitzHugh-Nagumo model very often considered in the context of studies on chimera states [4,17–19,25,29,40]. In what follows, the network behavior is explored numerically (with $N = 300$) with the help of certain characterization tools, with respect to the following control parameters: the coupling strength σ , the coupling range or coupling radius $r = R/N$, and the coupling phase ϕ . The initial conditions are randomly distributed on the circle of radius equal to 2 (i.e., $[u_k(0)]^2 + [v_k(0)]^2 = 4$), with an increasing density as $|\tan^{-1}[v_k(0)/u_k(0)]|$ gets closer to $\pi/2$ (see Fig. 1).

III. NETWORK BEHAVIOR: CHARACTERIZATION TOOLS AND NUMERICAL SIMULATION RESULTS

A quantitative measure, namely the strength of incoherence S was introduced [49] (with some corrections in Ref. [50]) to distinguish various collective dynamical states according to their degree of spatial incoherence. The strength of incoherence is a global order parameter based on the local standard deviation given by:

$$\sigma_m = \left\langle \sqrt{\frac{1}{n} \sum_{j=n(m-1)+1}^{mn} [z_j - \langle z \rangle_m]^2} \right\rangle_t, \tag{2}$$

where $n = N/M$, M is the number of bins of oscillators of equal size n , $m = 1, 2, \dots, M$, $z_j = u_j - u_{j+1}$, $\langle z \rangle_m = [\sum_{j=n(m-1)+1}^{mn} z_j]/n$, and $\langle \cdot \rangle_t$ denotes the time average. Then the strength of incoherence was introduced as:

$$S = 1 - \frac{\sum_{m=1}^M H(\sigma_{th} - \sigma_m)}{M}, \tag{3}$$

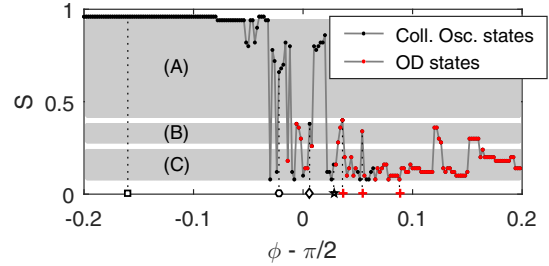


FIG. 2. The strength of incoherence S versus the coupling phase ϕ for $\sigma = 0.30$ and $r = 134/300 \approx 0.447$. The black dots denote collective oscillatory (Coll. Osc.) states and red dots for oscillation death (OD) states. The markers on the ϕ axis show the values of ϕ used to illustrate the prominent dynamical regimes: the square for Fig. 3, the diamond for Fig. 4, the circle for Fig. 5, the star for Fig. 6(b), and + for Fig. 7. The gray areas show the range of S for three distinct chimera states: (A) for the chimera state shown in Fig. 5, (B) for the chimera state shown in Fig. 4, and (C) for the chimera state shown in Fig. 6. As noted in the text, $\varepsilon = 0.1$, $\delta = 0.8$, $\gamma = 0.7$, and $I = -0.5$.

where $H(\cdot)$ is the Heaviside function and σ_{th} is a predefined threshold. The strength of incoherence $S \approx 1$ for incoherent patterns including spatial chaos and totally incoherent oscillation death states, $S = 0$ for fully coherent patterns like the in-phase synchronized state, and S has intermediate values between 0 and 1 for hybrid states including chimera states, solitary states, chimera death states, and other partially incoherent oscillation death states. When the network is in the oscillation death regime, small values of S may characterize cluster oscillation death states. As the strength of incoherence is no longer of any use in making the distinction between collective oscillatory states and oscillation death states, we use the intrinsic properties of the corresponding time series of u_k , $k = 1, 2, \dots, N$, with an emphasis on oscillation death states for which $u_k(t) \approx u_+$ for certain values of k and $u_k(t) \approx u_-$ for the other values of k , where u_+ and u_- are constant values that characterize the two branches of the oscillation death state.

In order to check whether the partially synchronous patterns characterized by $0 < S < 1$ are classical phase chimeras or not, we use the mean phase velocity profile $\{\omega_k = 2\pi M_k/\Delta t, k = 1, 2, \dots, N\}$, where M_k is the number of oscillation periods performed by the k th oscillator in the time interval Δt [40]. The mean phase velocity profile is typically arc shaped for incoherence with respect to the phase, while it is flat for coherence of phases.

Figure 2 shows the variations of the strength of incoherence S with respect to the coupling phase ϕ for $\sigma = 0.30$ and $r = 134/300$. This figure shows that there is a transition from incoherent oscillatory states (black dots with $S \approx 1$) to partially incoherent oscillation death states (red dots) via chimera states (black dots with $0 < S < 1$).

The totally incoherent collective oscillatory state depicted in Fig. 3 is characterized by spatial random swings between two periodic attractors; this is why we will refer to it as spatial chaos. Indeed Figs. 3(b) and 3(d) shows that the dynamics of all the oscillators is confined to two periodic attractors except for one oscillator ($k = 222$) whose dynamics evolves on a

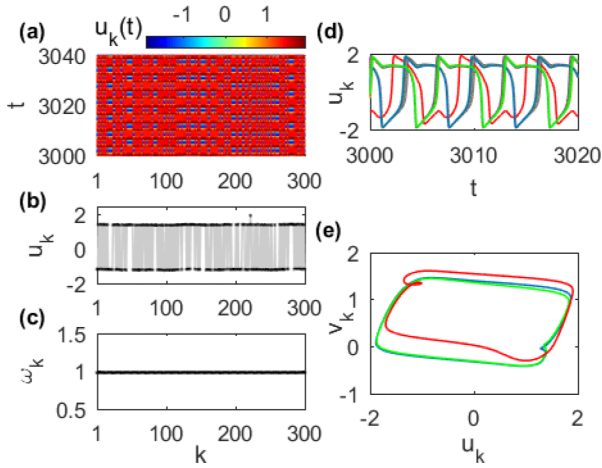


FIG. 3. Spatial chaos obtained for $\sigma = 0.30$, $r = 134/300 \approx 0.447$, and $\phi = \pi/2 - 0.160$: (a) space-time plot for the variable u ; (b) snapshot at $t = 3008.8$; (c) mean phase velocity profile; (d) time series $u_k(t)$ for all the oscillators, i.e., for $k = 1, 2, \dots, N$; (e) phase portraits $[u_k(t), v_k(t)]$ of three oscillators corresponding to the three periodic attractors shown in (d). As shown in (b), the oscillator $k = 222$ breaks away from the two characteristic clusters represented by the periodic attractors depicted by blue and green curves in (d) and (e); the dynamics of this solitary oscillator is depicted by red curves in (d) and (e). The gray lines in the snapshot serve as a guide to the eye. Other parameters as in Fig. 2.

different periodic attractor. All the three attractors mentioned have the same period, which is confirmed by the mean phase velocity profile shown in Fig. 3(c). The spatial chaos shown in Fig. 3 looks similar to the spatial phase-flip instability observed in the behavior of a network of identical Rössler oscillators interacting through a dynamic environment [50]. In this case, the oscillators undergo a random segregation into two clusters whose characteristic oscillations are antiphase. In the case shown in Fig. 3, even if the two periodic attractors characterizing the two clusters almost merge in the phase space [see Fig. 3(e)], their oscillations are not exactly antiphase because their phase lag is a bit less than π . This type of spatial chaos pattern was observed in networks of FitzHugh-Nagumo oscillators under the effect of time delay [4,46,47] and was identified as a partially synchronized salt-and-pepper state. In a salt-and-pepper state, due to a short wavelength instability [45] all the nodes oscillate with the same phase velocity but they are incoherently distributed between two slightly different states with constant phase lag [47]. There is also some resemblance to spatial chaos patterns found in networks of identical chaotic systems (logistic maps and Lorenz systems) with nonlocal coupling [38].

Now, with increasing value of the coupling phase ϕ , prominent clusters of synchronized oscillators may appear spontaneously in this form of spatial chaos giving rise to a novel form of chimera state illustrated in Fig. 4. The incoherent regions of this chimera pattern are characterized by the spatial random swings between a few periodic attractors (three in the case depicted in Fig. 4) that have the same period [see Fig. 4(c)]. Thereafter, we will refer to this type of chimera as type-1 chimera. This chimera state belongs to the class of “s-chimera” states [33–35], as the incoherent cluster is in a

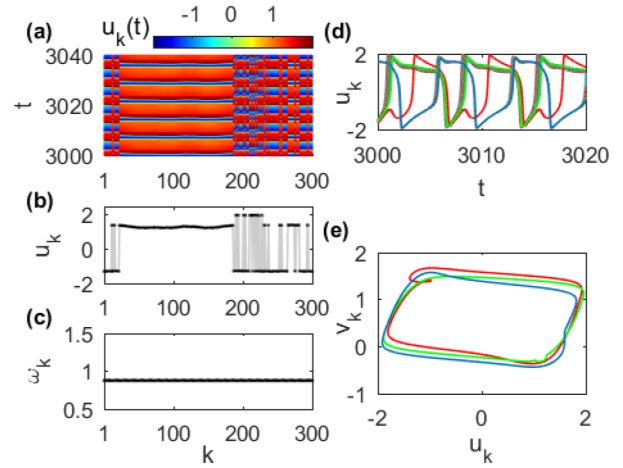


FIG. 4. Chimera state obtained for $\sigma = 0.30$, $r = 134/300 \approx 0.447$, and $\phi = \pi/2 + 0.006$: (a) space-time plot for the variable u ; (b) snapshot at $t = 3003.6$; (c) mean phase velocity profile; (d) time series $u_k(t)$ for all the oscillators, i.e., for $k = 1, 2, \dots, N$; and (e) phase portraits $[u_k(t), v_k(t)]$ of three oscillators corresponding to the three periodic attractors shown in (d). The gray lines in the snapshot serve as a guide to the eye. Other parameters as in Fig. 2.

spatial chaos regime. It is worthwhile to point out that the spatial chaos in the incoherent regions of this type-1 chimera pattern is more complex than the one of the totally incoherent state shown in Fig. 3 in that it involves three different attractors that do not merge in the phase space [see Fig. 4(e)]. Also, this is a novel chimera state that should not be confused with the solitary state chimera whose incoherent region is a solitary state, i.e., an ensemble of solitary nodes that are localized in space [17].

Type-1 chimera states are very rare. Indeed for the chosen set of parameters and the ϕ step used for Fig. 2, only one value of ϕ gives rise to this chimera [the only thick black dot in region (B) in Fig. 2]. This is due to the fact that very often some oscillators with solitary dynamics appear in the synchronous cluster. So, one obtains another chimera pattern with solitary nodes as shown in Fig. 5 where we can see that all the oscillators including the solitary ones have the same period [see Fig. 5(c)], which is a feature of solitary states and solitary state chimeras in coupled FitzHugh-Nagumo oscillators [17]. This second type of chimera that we will refer to as type-2 chimera corresponds to region (A) in Fig. 2. This “s-chimera” involving a solitary state is observed for the first time.

Another chimera with the lowest degree of incoherence [corresponding to region (C) in Fig. 2] emerges abundantly, we call it type-3 chimera which is nothing but the classical chimera observed in the earlier studies. Two examples of this type-3 chimera state are shown in Fig. 6 where we can notice arc-shaped patches in the mean phase velocity profile as a signature of classical chimeras. As shown in this figure, the size of the incoherent regions decreases with increasing value of the coupling range r , in such a way that for high value of r , this chimera pattern appears as a cluster synchronized state.

Besides the collective oscillatory states, the network exhibits various oscillation death states (steady states) that occur

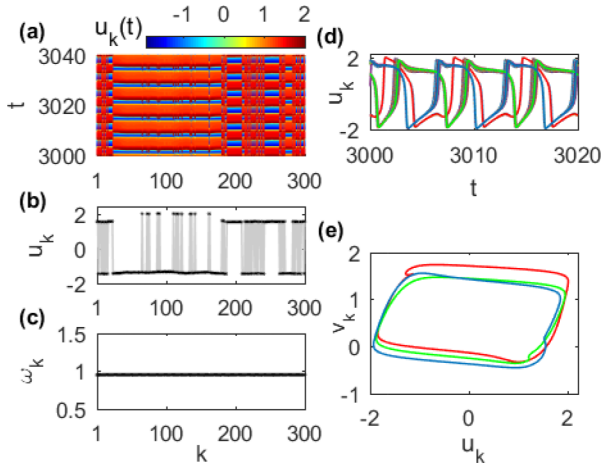


FIG. 5. Chimera pattern with solitary state obtained for $\sigma = 0.30$, $r = 134/300 \approx 0.447$, and $\phi = \pi/2 - 0.022$: (a) space-time plot for the variable u ; (b) snapshot at $t = 3008.2$; (c) mean phase velocity profile; (d) time series $u_k(t)$ for all the oscillators, i.e., for $k = 1, 2, \dots, N$; and (e) phase portraits $(u_k(t), v_k(t))$ of three oscillators corresponding to the three periodic attractors shown in (d). The coherent background and the incoherent clusters are ruled by the two attractors depicted by blue and green lines in (d) and (e) while the solitary oscillators dynamics is represented by the attractor depicted by red lines. The gray lines in the snapshot serve as a guide to the eye. Other parameters as in Fig. 2.

at higher values of the coupling phase ϕ as shown in Fig. 2. Among the plethora of oscillation death patterns observed, some particular ones retain our attention, namely chimera death states and coherent oscillation death states. Some examples of these patterns are shown in Fig. 7 where the number of clusters in a pattern refers to the number of uniform coherent domains. However, the number of clusters does not increase systematically following a clear bifurcation scenario as in Refs. [8,51,52].

Using the above characterization tools and arguments, the prominent dynamical regimes occurring in the network of FitzHugh-Nagumo oscillators are mapped in the coupling parameter space as shown in Fig. 8. One can notice that there are no clear boundaries between the dynamical states due to

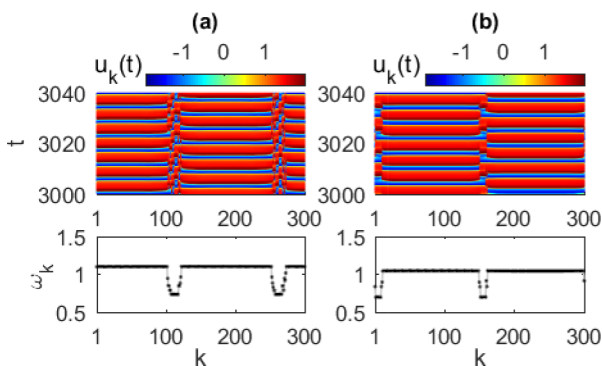


FIG. 6. Space-time plots and corresponding mean phase velocity profiles showing chimera patterns obtained for $\sigma = 0.30$: (a) $r = 120/300 = 0.400$ and $\phi = \pi/2 - 0.102$; (b) $r = 134/300 \approx 0.447$ and $\phi = \pi/2 + 0.028$. Other parameters as in Fig. 2.

high multistability. However, there is predominance of each state in a certain region of the parameter space. Overall, there is a transition from totally incoherent collective oscillatory states (spatial chaos) to partially coherent oscillation death states (including chimera death states) via chimera states. This overview confirms the rare occurrence of type-1 chimera states and the abundance of type-2 chimera states.

It would be interesting to verify the results summarized in Fig. 8 from a statistical point of view. To do so, the coupled system equations are solved repeatedly for a large number of arbitrarily chosen initial conditions of the same type, and the probability of obtaining each possible state is evaluated as the total number of occurrences of this state normalized to the total number of sets of initial conditions. For this statistical analysis, we consider 50 sets of initial conditions of the same type as those of Fig. 1, and we obtain the empirical probabilities shown in Fig. 9 for $r = 134/300 \approx 0.447$. For this value of r and for a given set of initial conditions, the behavior of the network can be read following the orange line in Fig. 8. Figure 9 confirms the prior results of Fig. 8, since each state is obtained with the highest probability in the region where it appears in Fig. 8. For example, spatial chaos is obtained with the maximum probability at low values of ϕ , while oscillation death (chimera death and coherent oscillation death) states are obtained with the maximum probability at high values of ϕ , and chimera states appear at intermediate values of ϕ . This statistical analysis demonstrates once more the rare occurrence of type-1 chimera.

Let us recall that for the above results, we have used a weighted distribution of initial conditions (see Fig. 1). It is worthwhile to point out that when the initial conditions follow a uniform random distribution as usually considered, we do not observe any chimera state—only oscillation death states are observed. In order to show how the chimera states disappear with decreasing inhomogeneity in the initial conditions, we still consider that the initial conditions $\{(u_k(0), v_k(0)), k = 1, 2, \dots, N\}$ are distributed on the circle with radius equal to 2, but now $u_k(0) = 2 \cos(\varphi_k)$ and $v_k(0) = 2 \sin(\varphi_k)$, where φ_k is an element of two superimposed Gaussian distributions with means $-\pi/2$ and $\pi/2$, respectively. The common standard deviation of the two Gaussian distributions σ_{gauss} is a control parameter that modulates the degree of inhomogeneity in the initial conditions. The degree of inhomogeneity decreases with increasing value of σ_{gauss} . Figure 10 shows two sets of initial conditions with different degrees of inhomogeneity, where the distribution is strongly weighted in (a) (as in Fig. 1), while it is “uniform” in (b). The network is statistically studied following the procedure described above, for $r \approx 0.447$ and $\phi = 0.006$, and for σ_{gauss} varying between the two values used for Fig. 10, i.e., $\sigma_{\text{gauss}} \in [0.6, 1.4]$. For the values of r and ϕ considered, the network has a nonzero probability to exhibit the two novel chimera states that are type-1 and type-2 chimera states (see the dashed gray line in Fig. 9). Figure 11 shows how the probabilities of obtaining the different dynamical states vary with respect to the degree of inhomogeneity in the initial conditions. As the degree of inhomogeneity decreases (σ_{gauss} increases from 0.6) the probability of obtaining spatial chaos states decreases while the probability of obtaining oscillation death states increases up to $\sigma_{\text{gauss}} \approx 1.0$. When the value of σ_{gauss} approaches unity, the

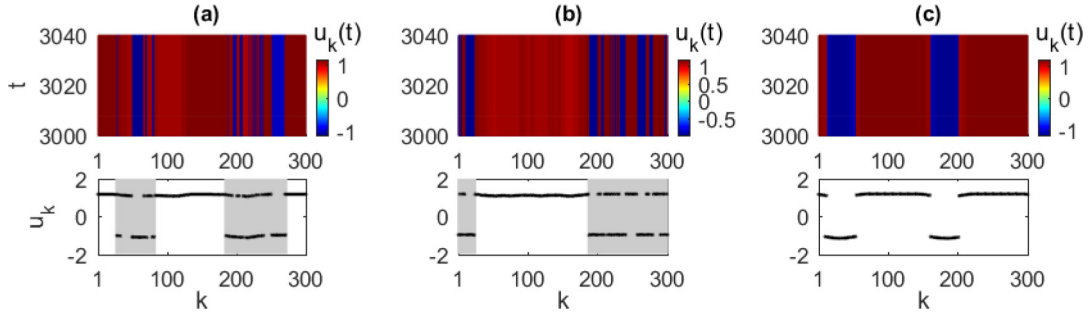


FIG. 7. Space-time plots and corresponding snapshots at $t = 3040$ showing some oscillation death states for $\sigma = 0.30$ and $r = 134/300 \approx 0.447$: (a) 2-cluster chimera death for $\phi = \pi/2 + 0.036$; (b) 1-cluster chimera death for $\phi = \pi/2 + 0.054$; (c) multicluster coherent oscillation death for $\phi = \pi/2 + 0.088$. The gray regions in the snapshots serve as guides to the eye for the visualization of the oscillation death incoherent regions. Other parameters as in Fig. 2.

probabilities of chimera states begin to decrease. Beyond the value $\sigma_{\text{gauss}} \approx 1.0$, the probability of oscillation death states approaches and reaches the value 1, while the probability of collective oscillatory states including chimera states approaches and reaches the value 0. This shows that the chimera states disappear when the initial conditions become uniform.

IV. BIFURCATION ANALYSIS OF OSCILLATION DEATH AND SOLITARY STATES IN A REDUCED MODEL

In order to explain the occurrence of oscillation death in networks of Stuart-Landau oscillators, the behavior of reduced models was analyzed in Refs. [51–53]. Here we perform a similar analysis for the FitzHugh-Nagumo system.

In oscillation death patterns, including chimera death patterns, certain oscillators populate the upper steady state branch characterized by u_+ and the others populate the lower steady state branch characterized by u_- . We introduce the new variables u_* and v_* as follows: $u_* = u_{\pm}$ characterizes any branch of the oscillation death state, and \bar{u}_* the other branch, i.e.,

$\bar{u}_* = u_-$ if $u_* = u_+$ and $\bar{u}_* = u_+$ if $u_* = u_-$. And the same reasoning for v_* and \bar{v}_* . Consider that $(u_k, v_k) = (u_*, v_*)$, then in Eq. (1) $u_j - u_k = 0$ (and $v_j - v_k = 0$) if the j th and k th units belong to the same branch of the oscillation death pattern, and otherwise $u_j - u_k = \bar{u}_* - u_*$ (and $v_j - v_k = \bar{v}_* - v_*$). Then, the network cluster populating the branch (u_*, v_*) is described by to the following equations:

$$\begin{aligned} v_* + u_* - \frac{u_*^3}{3} + I + \sigma' [b_{uu}(\bar{u}_* - u_*) + b_{uv}(\bar{v}_* - v_*)] &= 0, \\ -u_* - \delta v_* + \gamma + \sigma' [b_{vu}(\bar{u}_* - u_*) + b_{vv}(\bar{v}_* - v_*)] &= 0, \end{aligned} \quad (4)$$

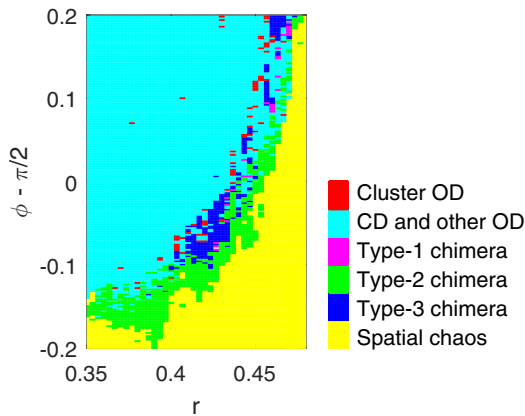


FIG. 8. Dynamical regimes map in the plane (coupling range r , coupling phase ϕ). Other parameters as in Fig. 2. OD and CD denote oscillation death and chimera death, respectively. By other OD, we mean other partially coherent OD states—totally incoherent OD states are unobserved. The orange line shows the value $r \approx 0.447$ used for Figs. 2 and 9.

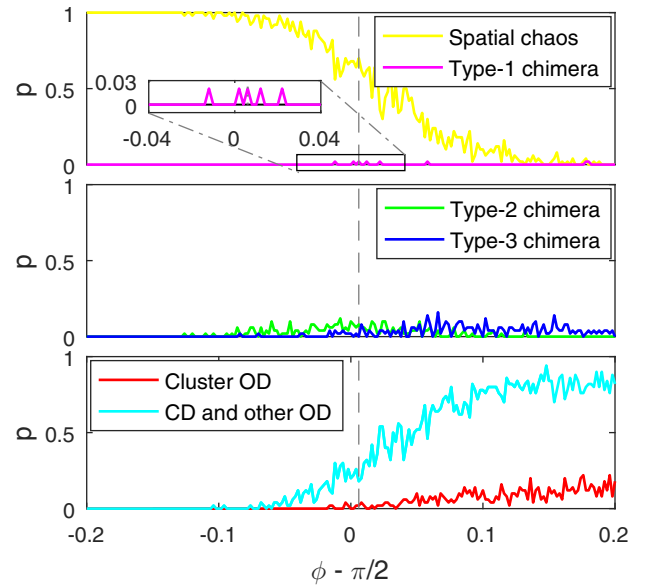


FIG. 9. Empirical probabilities p of obtaining the different dynamical states versus coupling phase ϕ , and other parameters as in Fig. 2 along the vertical orange line in Fig. 8. OD and CD denote oscillation death and chimera death, respectively. The color code is the same as in Fig. 8. The vertical dashed gray line shows the value $\phi = 0.006$ used for Fig. 11.

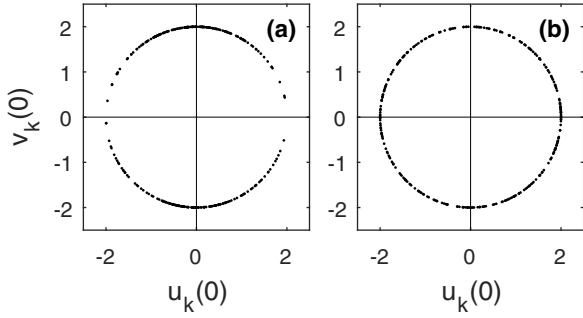


FIG. 10. Initial conditions obtained with two superimposed Gaussian distributions with peaks at $\tan^{-1}[v_k(0)/u_k(0)] = -\pi/2$ and $\pi/2$, and with a common standard deviation σ_{gauss} : (a) $\sigma_{\text{gauss}} = 0.6$ and (b) $\sigma_{\text{gauss}} = 1.4$.

where

$$\sigma' = \frac{\sum_{j=k-R}^{k+R} \delta_{j,k}}{2R} \sigma, \quad (5)$$

with

$$\delta_{j,k} = \begin{cases} 0 & \text{if } (u_j, v_j) = (u_k, v_k) = (u_*, v_*), \\ 1 & \text{if } (u_j, v_j) = (\bar{u}_*, \bar{v}_*) \neq (u_k, v_k). \end{cases}$$

Note that the value of the sum $\sum_{j=k-R}^{k+R} \delta_{j,k}$ in the formula of σ' depends on k and on the considered oscillation death pattern. However, regardless of the considered k and oscillation death pattern, $0 \leq \sum_{j=k-R}^{k+R} \delta_{j,k} \leq 2R$, so $0 \leq \sigma' \leq \sigma$. By analogy, the network cluster populating the branch (\bar{u}_*, \bar{v}_*) is

described by:

$$\begin{aligned} \bar{v}_* + \bar{u}_* - \frac{\bar{u}_*^3}{3} + I + \sigma' [b_{uu}(u_* - \bar{u}_*) + b_{uv}(v_* - \bar{v}_*)] &= 0, \\ -\bar{u}_* - \delta \bar{v}_* + \gamma + \sigma' [b_{vu}(u_* - \bar{u}_*) + b_{vv}(v_* - \bar{v}_*)] &= 0, \end{aligned} \quad (6)$$

It is worthwhile to point out that the set of equations given by Eqs. (4) and (6) is identical to the set of those describing oscillation death in a system of two FitzHugh-Nagumo oscillators coupled in the same way as in the considered network (with the only difference that the coupling strength is equal to σ'), namely:

$$\begin{aligned} \varepsilon \frac{du_k}{dt} &= v_k + u_k - \frac{1}{3} u_k^3 + I + \sigma' [b_{uu}(u_j - u_k) \\ &\quad + b_{uv}(v_j - v_k)], \\ \frac{dv_k}{dt} &= -u_k - \delta v_k + \gamma + \sigma' [b_{vu}(u_j - u_k) + b_{vv}(v_j - v_k)], \end{aligned} \quad (7)$$

where j and $k = 1, 2$, and $j \neq k$. Thus, studying the oscillation death phenomenon in the considered network would amount to studying oscillation death in this system of two coupled oscillators [52,53]. Each equilibrium point of Eq. (7) is given by the set $E = \{(u_{1*}, v_{1*}), (u_{2*}, v_{2*})\}$. An oscillation death state is characterized by the set $E = \{(u_+, v_+), (u_-, v_-)\}$ or $E = \{(u_-, v_-), (u_+, v_+)\}$, where (u_+, v_+) represents the upper branch of the oscillation death state, and (u_-, v_-) the lower branch. The equilibrium points of Eq. (7) and their bifurcations are investigated with the help of the Matlab continuation toolbox Matcont [54], and the results are depicted in Fig. 12 for $0 \leq \sigma' \leq \sigma = 0.30$ as justified above. Figure 12(a) shows that for small values of σ' , the system of two coupled oscillators has only one equilibrium point $E_0 = \{(u_0, v_0), (u_0, v_0)\}$. This only equilibrium point is unstable and is surrounded by a stable limit cycle, which corresponds to oscillatory behavior in the coupled system. As the value of σ' increases, E_0 undergoes a subcritical pitchfork bifurcation giving rise to two new unstable equilibrium points. The two new branches gain stability via a fold bifurcation of equilibria on the one hand and a subcritical Hopf bifurcation on the other hand. These two branches are given by $E_1 = \{(u_+, v_+), (u_-, v_-)\}$ and $E_2 = \{(u_-, v_-), (u_+, v_+)\}$, which is typical of the oscillation death phenomenon. We obtain the same bifurcation scenario with respect to ϕ [see Fig. 12(b)]. Overall, Fig. 12 shows that the oscillation death phenomenon can occur in the system of two coupled FitzHugh-Nagumo oscillators, which justifies the occurrence of oscillation death states in the considered network, on the basis of the similarity between Eqs. (4) and (6) on the one hand and the equations describing Eq. (7) equilibrium points on the other hand. Note that for the other values of ϕ in $[\pi/2 - 0.2, \pi/2 + 0.2]$ as considered in Fig. 8, the results shown in Fig. 12 do not change significantly. However, it can happen that a stable limit cycle and stable equilibrium points $E_1 = \{(u_+, v_+), (u_-, v_-)\}$ and $E_2 = \{(u_-, v_-), (u_+, v_+)\}$ coexist, underlining the coexistence of collective oscillatory behavior and oscillation death states in the network. The fact that there might exist Hopf bifurcations triggering the formation of new limit cycles at

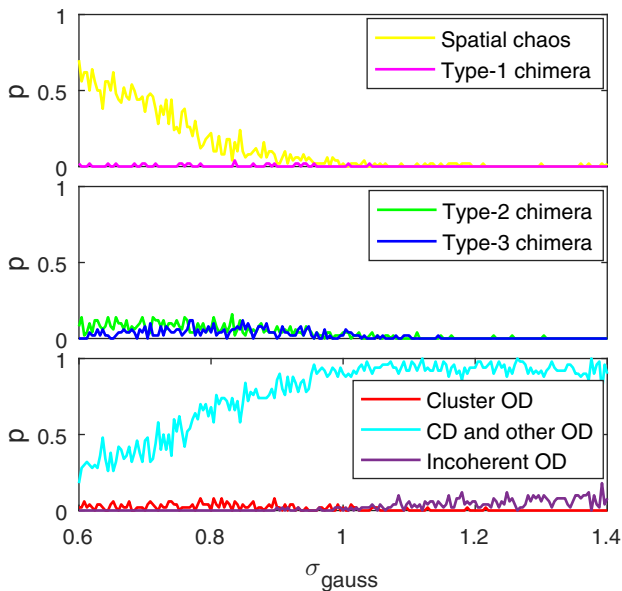


FIG. 11. Empirical probabilities of obtaining the different dynamical states versus σ_{gauss} measuring the degree of inhomogeneity in the initial conditions, for $r \approx 0.447$, $\phi = 0.006$, and other parameters as in Fig. 2. OD and CD denote oscillation death and chimera death, respectively. The color code is the same as in Fig. 8.

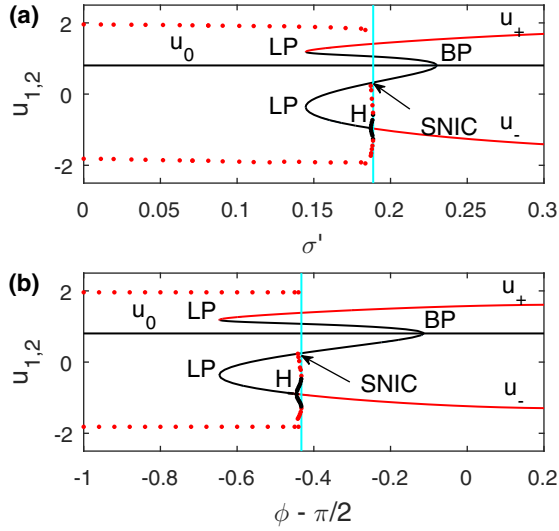


FIG. 12. Bifurcation diagram of the reduced system [Eq. (7)] with respect to the coupling strength σ' (a) for $\phi = \pi/2 + 0.05$, and with respect to the coupling phase ϕ (b) for $R = 126$ (i.e., $r = 0.42$) and $\sum_{j=k-R}^{k+R} \delta_{j,k} = 210$ in the formula of σ' given by Eq. (5). Other parameters as in Fig. 2. Red (respectively, black) lines indicate stable (respectively, unstable) steady states. Red (respectively, black) dots represent the amplitudes of stable (respectively, unstable) limit cycles. The cyan line (going through the folds of cycles originating from the Hopf bifurcation labeled H) marks the threshold between oscillatory behavior (on the left) and oscillation death behavior (on the right). LP, BP, and SNIC denote limit point (also known as fold of equilibria), branching point (also known as pitchfork bifurcation) and saddle-node on invariant circle bifurcation, respectively.

the transition from oscillation death to oscillatory behavior in the system of two coupled oscillators, would explain the multistability responsible for the formation of solitary states in chimera patterns at the transition from spatial chaos to oscillation death states in the network. This chimera with solitary state exists in a small region of the parameter space because the newly created limit cycles would exist only in a small region of the parameter space as they rapidly vanish via saddle-node on invariant circle (SNIC) bifurcations as shown in Fig. 12.

Furthermore, the bifurcation analysis of the reduced system by Eq. (7) can help explaining the shape of the boundary given in Fig. 8 between collective oscillatory states and oscillation death states in the plane (r, ϕ) . Indeed, this boundary looks like a simple curve. To do so, a two-parameter bifurcation diagram in the plane (r, ϕ) is derived from the one-parameter bifurcation diagram shown in Fig. 12(b). The result is shown in Fig. 13, where we can see that the Hopf bifurcation curves have the same shape as the boundary between oscillatory states and oscillation death states in Fig. 8. We should remember that this Hopf bifurcation is in close proximity to the folds of cycles marking the threshold between

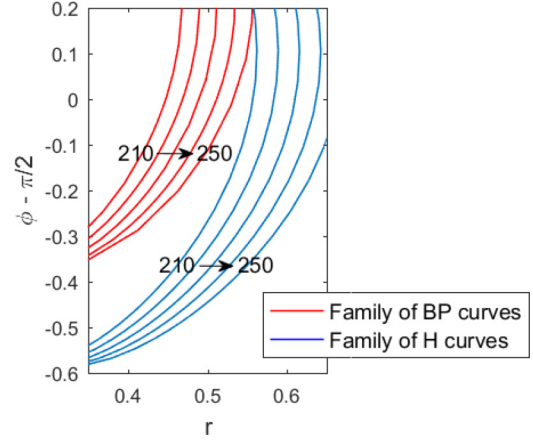


FIG. 13. Codimension-two bifurcation diagram of the reduced system [Eq. (7)] with respect to the coupling range r and coupling phase ϕ . The bifurcation curves are obtained for different values of the sum $\sum_{j=k-R}^{k+R} \delta_{j,k}$ in the formula of σ' given by Eq. (5), $\sum_{j=k-R}^{k+R} \delta_{j,k} = 210, 220, 230, 240, \text{ and } 250$. Other parameters as in Fig. 2. BP for branch point (pitchfork) bifurcation and H for Hopf bifurcation.

oscillatory states and oscillation death states in the reduced system (see Fig. 12).

V. CONCLUSION

A network of the original FitzHugh-Nagumo model in the presence of a stimulus has been studied in the context of symmetry-breaking phenomena. It has been found that this network exhibits diverse symmetry-breaking patterns including classical chimera states and two novel chimera states. Apart from those oscillatory states, a plethora of partially coherent oscillation death states have been identified, such as chimera death and multicluster coherent oscillation death states. The oscillators in the patterns of these novel chimeras evolve on a few fixed periodic attractors; the incoherent region being characterized by spatial random swings between these few periodic attractors. The coherent region of the simplest of these chimera patterns is characterized by total coherence. However, very often some oscillators with identical solitary dynamics appear in the coherent region of this chimera pattern giving rise to a more complicated pattern. Finally, we have explained the occurrence of oscillation death based on the bifurcation scenarios of the reduced model of the network. The bifurcation diagram of equilibrium points of the reduced two-oscillator system shows that there might exist Hopf bifurcations creating new limit cycles at the transition from oscillation death to oscillatory behavior, which would help explaining the multistability underlying the formation of chimeras with solitary states at the transition from spatial chaos to oscillation death states in the considered network. Our study reveals that the original FitzHugh-Nagumo model in the presence of a stimulus can give rise to several exotic states that are not exhibited by the simplified models.

- [1] S. Strogatz, *Sync: The Emerging Science of Spontaneous Order* (Hyperion, New York, 2003).
- [2] A. Pikovsky, M. Rosenblum, and J. Kurths, *Synchronization: A Universal Concept in Nonlinear Science* (Cambridge University Press, Cambridge, UK, 2001).
- [3] S. Boccaletti, A. N. Pisarchik, C. I. del Genio, and A. Amann, *Synchronization: From Coupled Systems to Complex Networks* (Cambridge University Press, Cambridge, UK, 2018).
- [4] A. Zakharova, *Chimera Patterns in Networks: Interplay between Dynamics, Structure, Noise, and Delay* (Springer Nature Switzerland AG, Cham, Switzerland, 2020).
- [5] A. Koseska, E. Volkov, and J. Kurths, *Phys. Rep.* **531**, 173 (2013).
- [6] B. Bandyopadhyay, T. Khatun, D. Biswas, and T. Banerjee, *Phys. Rev. E* **102**, 062205 (2020).
- [7] W. Zou, D. V. Senthilkumar, M. Zhan, and J. Kurths, *Phys. Rep.* **931**, 1 (2021).
- [8] A. Zakharova, M. Kapeller, and E. Schöll, *Phys. Rev. Lett.* **112**, 154101 (2014).
- [9] Y. Maistrenko, B. Penkovsky, and M. Rosenblum, *Phys. Rev. E* **89**, 060901(R) (2014).
- [10] P. Jaros, S. Brezetsky, R. Levchenko, D. Dudkowsky, T. Kapitaniak, and Y. Maistrenko, *Chaos* **28**, 011103 (2018).
- [11] H. Taher, S. Olmi, and E. Schöll, *Phys. Rev. E* **100**, 062306 (2019).
- [12] F. Hellmann, P. Schultz, P. Jaros, R. Levchenko, T. Kapitaniak, J. Kurths, and Y. Maistrenko, *Nat. Commun.* **11**, 592 (2020).
- [13] R. Berner, A. Polanska, E. Schöll, and S. Yanchuk, *Eur. Phys. J. Spec. Top.* **229**, 2183 (2020).
- [14] I. Franović, S. Eydram, N. Semenova, and A. Zakharova, *Chaos* **32**, 011104 (2022).
- [15] M. Mikhaylenko, L. Ramlow, S. Jalan, and A. Zakharova, *Chaos* **29**, 023122 (2019).
- [16] E. Rybalova, G. I. Strelkova, and V. S. Anishchenko, *Chaos Soliton. Fract.* **115**, 300 (2018).
- [17] E. Rybalova, V. S. Anishchenko, G. I. Strelkova, and A. Zakharova, *Chaos* **29**, 071106 (2019).
- [18] E. Schöll, *Europhys. Lett.* **136**, 18001 (2021).
- [19] L. Kang, C. Tian, S. Huo, and Z. Liu, *Sci. Rep.* **9**, 14389 (2019).
- [20] N. C. Rattenborg, C. J. Amlaner, and S. L. Lima, *Neurosci. Biobehav. Rev.* **24**, 817 (2000).
- [21] N. C. Rattenborg, B. Voirin, S. M. Cruz, R. Tisdale, G. Dell’Omo, H. P. Lipp, M. Wikelski, and A. L. Vyssotski, *Nat. Commun.* **7**, 12468 (2016).
- [22] P. Tass, M. G. Rosenblum, J. Weule, J. Kurths, A. Pikovsky, J. Volkman, A. Schnitzler, and H.-J. Freund, *Phys. Rev. Lett.* **81**, 3291 (1998).
- [23] M. Gerster, R. Berner, J. Sawicki, A. Zakharova, A. Škoch, J. Hlinka, K. Lehnertz, and E. Schöll, *Chaos* **30**, 123130 (2020).
- [24] S. Majhi, B. K. Bera, D. Ghosh, and M. Perc, *Phys. Life Rev.* **28**, 100 (2019).
- [25] T. Chouzouris, I. Omelchenko, A. Zakharova, J. Hlinka, P. Jiruska, and E. Schöll, *Chaos* **28**, 045112 (2018).
- [26] R. G. Andrzejak, C. Rummel, F. Mormann, and K. Schindler, *Sci. Rep.* **6**, 23000 (2016).
- [27] R. Curtu, *Physica D* **239**, 504 (2010).
- [28] D. S. Bassett, P. Zurn, and J. I. Gold, *Nat. Rev. Neurosci.* **19**, 566 (2018).
- [29] Z. Wang and Z. Liu, *Front. Physiol.* **11**, 724 (2020).
- [30] E. M. Izhikevich, *Dynamical Systems in Neuroscience: The Geometry of Excitability and Bursting* (The MIT Press, Cambridge, MA, 2007).
- [31] Y. Kuramoto and D. Battogtokh, *Nonlin. Phenom. Complex Syst.* **5**, 380 (2002).
- [32] D. M. Abrams and S. H. Strogatz, *Phys. Rev. Lett.* **93**, 174102 (2004).
- [33] D. Dudkowsky, Y. Maistrenko, and T. Kapitaniak, *Phys. Rev. E* **90**, 032920 (2014).
- [34] A. Mishra, C. Hens, M. Bose, P. K. Roy, and S. K. Dana, *Phys. Rev. E* **92**, 062920 (2015).
- [35] D. Dudkowsky, Y. Maistrenko, and T. Kapitaniak, *Chaos* **26**, 116306 (2016).
- [36] F. Parastesh, S. Jafari, H. Azarnoush, Z. Shahriari, Z. Wang, S. Boccaletti, and M. Perc, *Phys. Rep.* **898**, 1 (2021).
- [37] I. Omelchenko, Y. Maistrenko, P. Hövel, and E. Schöll, *Phys. Rev. Lett.* **106**, 234102 (2011).
- [38] I. Omelchenko, B. Riemenschneider, P. Hövel, Y. Maistrenko, and E. Schöll, *Phys. Rev. E* **85**, 026212 (2012).
- [39] A. M. Hagerstrom, T. E. Murphy, R. Roy, P. Hövel, I. Omelchenko, and E. Schöll, *Nat. Phys.* **8**, 658 (2012).
- [40] I. Omelchenko, O. E. Omel’chenko, P. Hövel, and E. Schöll, *Phys. Rev. Lett.* **110**, 224101 (2013).
- [41] N. Semenova, A. Zakharova, V. Anishchenko, and E. Schöll, *Phys. Rev. Lett.* **117**, 014102 (2016).
- [42] A. Zakharova, N. Semenova, V. Anishchenko, and E. Schöll, Noise-induced chimera states in a neural network, in *Patterns of Dynamics*, Springer Proceedings in Mathematics and Statistics, Vol. 205, edited by P. Gurevich, J. Hell, B. Sandstede, and A. Scheel (Springer, Cham, 2017), pp. 44–63.
- [43] N. Semenova, *Eur. Phys. J. Spec. Top.* **229**, 2295 (2020).
- [44] L. Schülen, A. Gerdes, M. Wolfrum, and A. Zakharova, *Phys. Rev. E* **106**, L042203 (2022).
- [45] C. Bachmair and E. Schöll, *Eur. Phys. J. B* **87**, 276 (2014).
- [46] J. Sawicki, I. Omelchenko, A. Zakharova, and E. Schöll, *Eur. Phys. J. B* **92**, 54 (2019).
- [47] J. Sawicki, J. M. Koulen, and E. Schöll, *Chaos* **31**, 073131 (2021).
- [48] R. FitzHugh, *Biophys. J.* **1**, 445 (1961).
- [49] R. Gopal, V. K. Chandrasekar, A. Venkatesan, and M. Lakshmanan, *Phys. Rev. E* **89**, 052914 (2014).
- [50] R. Gopal, V. K. Chandrasekar, D. V. Senthilkumar, A. Venkatesan, and M. Lakshmanan, *Commun. Nonlinear Sci. Numer. Simulat.* **59**, 30 (2018).
- [51] S. G. Ngueuteu Mbouna, T. Banerjee, R. Yamapi, and P. Wofo, *Chaos Soliton. Fract.* **157**, 111945 (2022).
- [52] I. Schneider, M. Kapeller, S. Loos, A. Zakharova, B. Fiedler, and E. Schöll, *Phys. Rev. E* **92**, 052915 (2015).
- [53] T. Banerjee, *Europhys. Lett.* **110**, 60003 (2015).
- [54] A. Dhooge, W. Govaerts, and Y. A. Kuznetsov, *ACM Trans. Math. Softw.* **29**, 141 (2003).